The Voltage-Gated Ca^{2+} Channel Is the Ca^{2+} Sensor Protein of Secretion[†]

Yamit Hagalili, Niv Bachnoff, and Daphne Atlas*

Department of Biological Chemistry, The Institute of Life Sciences, The Hebrew University of Jerusalem, Jerusalem, 91904 Israel

Received June 19, 2008; Revised Manuscript Received November 17, 2008

ABSTRACT: Neurotransmitter release involves two consecutive Ca^{2+}-dependent steps, an initial Ca^{2+} binding to the selectivity filter of voltage-gated Ca^{2+} channels (VGCC) followed by Ca^{2+} binding to synaptic vesicle protein. The unique Ca^{2+}-binding site of the VGCC is located within the α_1 subunit of the Ca^{2+} channel. The structure of the selectivity filter allows for the binding of Ca^{2+}, Sr^{2+}, Ba^{2+}, and La^{3+}. Despite its cell impermeability, La^{3+} supports secretion, which is in contradistinction to the commonly accepted mechanism in which elevation of cytosolic ion concentrations ($[Ca^{2+}]_i$) and binding to synaptotagmin(s) trigger release. Here we show that a Cav1.2-mutated $\alpha_1$1.2/L775P subunit which does not conduct Ca^{2+} currents supports depolarization-evoked release by means of Ca^{2+} binding to the pore. Bovine chromaffin cells, which secrete catecholamine almost exclusively via nifedipine-sensitive Cav1.2, were infected with the Semliki Forest Virus, pSFV $\alpha_1$1.2/L775P. This construct also harbored a second mutation that rendered the channel insensitive to nifedipine. Depolarization of cells infected with $\alpha_1$1.2/L775P triggered release in the presence of nifedipine. Thus, the initial Ca^{2+} binding at the pore of the channel appeared to be sufficient to trigger secretion, indicating that the VGCC could be the primary Ca^{2+} sensor protein. The 25% lower efficiency, however, implied that additional ancillary effects of elevated $[Ca^{2+}]_i$ were essential for optimizing the overall release process. Our findings suggest that the rearrangement of Ca^{2+} ions within the pore of the channel during membrane depolarization triggers secretion prior to Ca^{2+} entry. This allows for a tight temporal coupling between the depolarization event and exocytosis of vesicles tethered to the channel.

The process of neurotransmitter release involves two distinct consecutive Ca^{2+} binding steps. Initially, Ca^{2+} binds to the voltage-gated Ca^{2+} channel (VGCC) and, subsequently, to the vesicular synaptotagmin and other intracellular Ca^{2+} sensors. The rise in cytosolic Ca^{2+} concentration and binding of Ca^{2+} to the C2A and C2B domains of either of the synaptotagmin isoforms have implicated synaptotagmin as the Ca^{2+} sensor of synaptic release and neuroendocrine secretion (*1*−*9*). The VGCC according to this model is considered as a vehicle for bringing Ca^{2+} into the cell. The possibility of a Ca^{2+}-bound channel serving as a potential Ca^{2+} sensor that triggers secretion is neglected in this model.

Ca^{2+} conductance through the channel involves Ca^{2+} binding to the EEEE locus, which is composed of four glutamates from each segment of the α_1 subunit of the Ca^{2+} channel and is known as the selectivity filter of the VGCC (*10*−*14*). The EEEE locus functions as a unique Ca^{2+}-binding site of the VGCC. This region of the pore limits and provides specificity for the passage of ions across the cell membrane (*10*−*14*). The structure adopted by the atoms at the channel pore is largely determined by the ionic radius and charge of the bound cations, constraining both ion binding and permeation. For example, the binding of Ca^{2+}, Sr^{2+}, Ba^{2+}, and La^{3+} is allowed, while the permeation of cation La^{3+} is restricted.

Recently, it was shown that despite being excluded from entry into the cell, La^{3+} by interacting with the VGCC in nominally Ca^{2+}-free solution supported depolarization-evoked catecholamine release in chromaffin cells, and glucose-induced insulin release in pancreatic β cells (*15*−*17*). Secretion driven by La^{3+} residing at the selectivity filter raised the possibility that the Ca^{2+} binding at the channel could also trigger release, prior to Ca^{2+} binding to vesicular proteins.

The association and the specific functional interactions of VGCC with the exocytotic proteins are consistent with a putative signaling role of a Ca^{2+}-bound channel in triggering secretion (*18*−*29*). Such regulation is attractive because it confines the trigger of release to a conformational switch within a tightly bound heteroprotein complex, prior to elevation of cytosolic Ca^{2+} concentrations (*18*−*29*).

To examine whether Ca^{2+} binding at the selectivity filter alone, without entry into the cell, is sufficient to trigger secretion, we studied a single-point-mutated channel, which rendered the channel impermeable to Ca^{2+} (*30*); in addition, the channel harbors a single-point mutation conferring nifedipine insensitivity to the channel.

We show that KCl-induced membrane depolarization could trigger secretion in chromaffin cells infected with $\alpha_1$1.2/L775P, the nonconducting mutated $\alpha_1$1.2 subunit of Cav1.2. The release was assayed in the presence of nifedipine which in these cells blocks ~90% of the release associated with

[†] Supported by the Betty Feffer Foundation (D.A.).

* To whom correspondence should be addressed: Institute of Life Sciences, Department of Biological Chemistry, The Hebrew University of Jerusalem, Jerusalem, 91904 Israel. Phone: 972-2658-5406. Fax: 972-2658 5413. E-mail: datlas@vms.huji.ac.il.

10.1021/bi801619f CCC: $40.75
Published on Web 12/05/2008

the endogenous channels. These results demonstrate that Ca^{2+} binding at the pore is necessary and sufficient to trigger catecholamine release prior to Ca^{2+} influx. Our findings suggest that the VGCC triggers release through relocation of Ca^{2+} ions at the EEEE locus, which in turn transmits its signal to the exocytotic machinery. Unlike previous results (*4, 31*), in this proposed model, the fast process occurs upstream from Ca^{2+} binding to vesicular synaptotagmin. This is consistent with the view that the Ca^{2+} channel serves as the Ca^{2+} sensor of secretion in chromaffin cells.

RESULTS

Cav1.2/L775P's Lack of Conductivity. We examined depolarization-evoked release using a cloned Cav1.2 in which the pore-forming subunit $\alpha_1$1.2 has been mutated to $\alpha_1$1.2/L775P (*30*). This mutation made the channel Ca^{2+} impermeable to Ca^{2+} influx (Figure 1A). The cRNAs encoding the GFP-tagged $\alpha_1$1.2 subunit of Cav1.2 or the GFP-$\alpha_1$1.2/L775P mutant were co-injected into oocytes along with the cRNAs encoding the auxiliary $\alpha 2\delta$ and β2A channel subunits. Oocytes were imaged by confocal microscopy and analyzed for inward currents using the two-electrode-voltage-clamp technique (*20, 22, 32*).

The confocal images demonstrated predominant targeting of both the control GFP-$\alpha_1$1.2 and mutated GFP-$\alpha_1$1.2/L775P to the cell membrane (Figure 1B, top), consistent with the cell membrane targeting of $\alpha_1$1.2/L775P, in human embryonic kidney tsA-20 cells (*30*). The addition of GFP fused to $\alpha_1$1.2 did not affect the electrophysiological kinetics of Cav1.2 (Figure 1 of the Supporting Information).

Cav1.2/L775P, as previously reported (*30*), failed to conduct current (Figure 1B, right) in contrast to a significant conduction of macroscopic whole-cell Ba^{2+} and Ca^{2+} currents, I_{Ba} and I_{Ca}, respectively, through Cav1.2 [Figure 1B, left (*20, 32*)]. These results were observed throughout the examined test potentials as shown by the superimposed current traces and current−voltage relationship (Figure 1C, bottom). In contrast, the three-channel subunits $\alpha_1$1.2/L775P/$\alpha 2\delta/\beta$2A behaved like $\alpha 2\delta/\beta$2A without the $\alpha_1$1.2 subunit and failed to conduct currents (Figure 1C). These results demonstrated the Ca^{2+} and Ba^{2+} impermeability of $\alpha_1$1.2/L775P, consistent with results obtained previously from patch-clamp recordings in tsA-20 cells (*30*).

The Cav1.2/L775P Channel Is Voltage-Gated, and the Cavity of the Mutated Channel Is Accessible to Extracellular Ca^{2+}. It is well-established that in the absence of extracellular Ca^{2+}, Cav1.2 conducts monovalent ions, Li^+ and Na^+, which bind with low affinity to the selectivity filter (*10, 33, 34*). In the absence of Ca^{2+} currents, the Li^+ conductance of Cav1.2 was used to confirm the voltage sensitivity and gating of $\alpha_1$1.2/L775P.

The Li^+ conductivity of Cav1.2 and Cav1.2/L775P expressed in oocytes is depicted by superimposed current traces (see above) (Figure 2A). Unlike a complete block of I_{Ca} and I_{Ba}, Cav1.2/L775P conducted Li^+ current (I_{Li}) with a significantly smaller amplitude (>100 fold), compared to I_{Li} in the control Cav1.2. The normalized current−voltage relationship of Cav1.2/L775P was shifted by 6 mV to negative potentials but clearly established the voltage dependency of the Ca^{2+}-impermeable channel (Figure 2B).

The blockade of the monovalent current by micromolar concentrations of Ca^{2+} has previously been used to identify the EEEE locus of Cav1.2 as a common binding site for the mono- and divalent cations (*10*). As shown in Figure 2C, I_{Li} through Cav1.2 and Cav1.2/L775P was virtually abolished by 50 μM Ca^{2+}, revealing Ca^{2+} binding at the Cav1.2/L775P selectivity filter.

Given a channel subunit, which is voltage-gated, binds Ca^{2+} at the pore, and is Ca^{2+}-impermeable, we examined its capacity to support depolarization-evoked release using amperometry recordings in bovine chromaffin cells.

To distinguish between our introduced channels and the endogenous cellular channels, our cloned channels were made resistant to nifedipine (Nif) by a single-amino acid mutation, T1066Y (*35, 36*). The Nif insensitivity was confirmed in microinjected oocytes where I_{Ca} through Cav1.2/T1066Y was conducted in the presence 5 μM nifedipine, compared to a complete current blockade in the normal Cav1.2 channel (Figure 2A,B of the Supporting Information).

Chromaffin Cells as an Assay for Monitoring Secretion via CaV1, the L-Type Channels. At first we investigated the fraction of depolarization-evoked release that could be blocked by nifedipine. Secretion and the fusion of single vesicles in chromaffin cells were monitored by amperometric currents using carbon fiber microelectrodes (*37*−*39*). Amperometric currents induced by 60 mM KCl (K60) in native noninfected cells (Figure 3A) were significantly reduced (~90%) by either 5 or 10 μM nifedipine added to the external solution (Figure 3, top middle, top right), consistent with previous reports (*15, 40*). The rate of secretion was quantified by a cumulative spike plot, in which spike counts were plotted versus time after K60 stimulation (Figure 3B). The total mean charge, which provides a read-out of total catecholamine secretion, was calculated as the sum of the total mean charge over time. The reduction in both the rate of secretion and total mean charge by nifedipine demonstrate the major contribution (90%) of Cav1 to secretion in these cells (Figure 3C). In contrast, the reduction in Fura-2 fluorescence elicited in chromaffin cells during K60 stimulation was only 25−30% (Figure 3D), consistent with the reduction in the intracellular calcium concentration ($[Ca^{2+}]_i$), previously published for these cells (*41, 42*) and in PC12 cells (*43*). The nifedipine-insensitive Ca^{2+} influx is mediated by non-Cav1 VGCCs, which supports ~10% of the release in bovine chromaffin cells (*44*).

The L775P Mutated Channel Supports Depolarization-Evoked Release in Chromaffin Cells. We then studied secretion mediated by nifedipine-insensitive mutants in the presence of 5 μM nifedipine.

The Nif-insensitive $\alpha_1$1.2 and $\alpha_1$1.2/L775P subunits were subcloned into a Semliki Forest viral vector pSFV, which expresses GFP through an internal ribosome entry site (IRES) motif.

At first we tested the effects of Semliki Forest virus infection on secretion. As shown in Figure 3A,B of the Supporting Information, there was no significant difference in the number of spikes or total catecholamine secretion (Figure 3C of the Supporting Information) between the noninfected and GFP-infected cells. The rate of secretion, which is shown as an average number of cumulative spike counts (Figure 3D of the Supporting Information), was

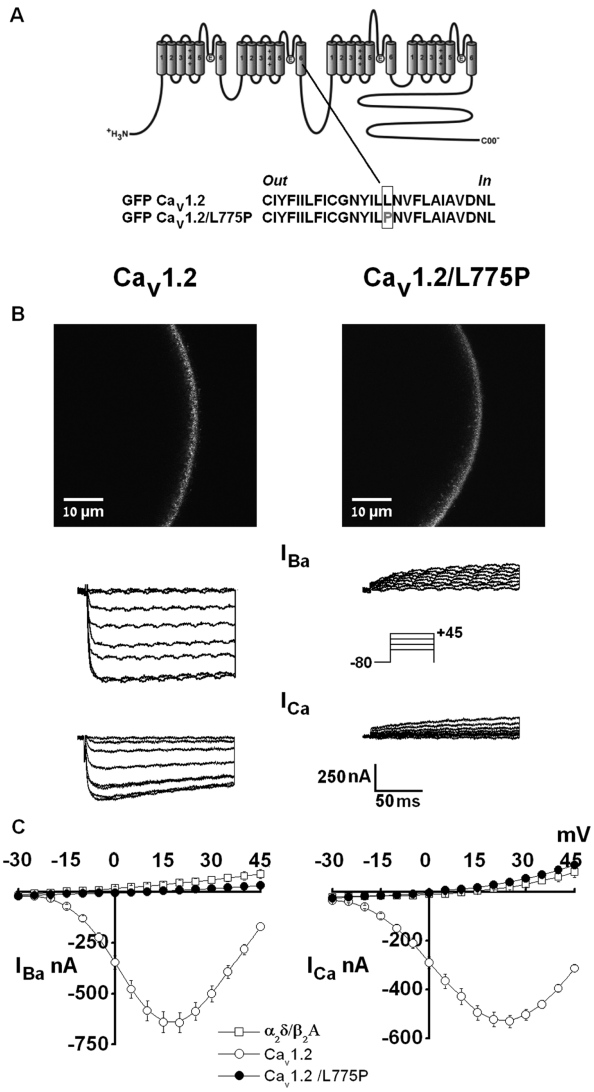

FIGURE 1: L775P-mutated Cav1.2 channel that is targeted to the cell membrane and is Ba^{2+}- and Ca^{2+}-impermeable. (A) Schematic location of L775P at IIS6 of the pore-forming $\alpha_1$1.2 subunit of Cav1.2. (B) cRNAs encoding the GFP-tagged $\alpha_1$1.2 subunit (4 ng/oocyte) were co-injected into oocytes along with the cRNAs encoding $\alpha 2\delta$ (4 ng/oocyte) and β2A (8 ng/oocyte) auxiliary channel subunits. Five days after injection, membrane targeting (top) and current conductance were tested (bottom). Membrane targeting of the α_1 subunits of Cav1.2 control and Cav1.2/L775P in oocytes. Confocal images of the GFP-tagged $\alpha_1$1.2 and GFP-tagged $\alpha_1$1.2 /L775P (10 ng/oocyte) show the location at the cell membrane in *Xenopus* oocytes expressing the corresponding channel subunits. Impermeability of Cav1.2/L755P. Macroscopic whole-cell Ba^{2+} currents (I_{Ba} and I_{Ca}) were elicited from a holding potential of −80 mV to various test potentials in response to a 200 ms test pulse (*15, 17*). Representative traces of $\alpha_1$1.2/$\alpha 2\delta/\beta$2A and $\alpha_1$1.2 (L775P)/$\alpha 2\delta/\beta$2A I_{Ba} (top) and I_{Ca} (Cav1.2) (bottom) evoked from a holding potential of −80 mV by a 200 ms pulse to various test potentials. The traces shown have been corrected for leakage and capacitive transients by online subtraction. (C) Leak-subtracted peak current−voltage relationships. Data collected from oocytes (n = 12−15) expressing $\alpha_1$1.2/$\alpha 2\delta/\beta$2A (○) as the control, $\alpha_1$1.2/L775P/$\alpha 2\delta/\beta$2A (●), and $\alpha 2\delta/\beta$2A subunits (○), in Ba^{2+} (left) and Ca^{2+} (right). $\alpha_1$1.2 (2 ng/oocyte) (*46*) and $\alpha_1$1.2/L775P (10 ng/oocyte) were co-injected together with $\alpha 2\delta$ (2 ng/oocyte) and β2A (2 ng/oocyte). The traces shown have been corrected for leakage and capacitative transients by online subtraction. The data points correspond to the mean ± the standard error of the mean of currents (n = 12−14). Two sample Student's t tests was applied, and p values of <0.001 were obtained from the two-tailed test.

slightly affected by the virus. The initial rate measured over 12 s after 60K stimulation was reduced from 0.76 ± 0.03 to 0.57 ± 0.001 spike/s in the infected cells, and the sustained rate measured in the time range of 23−40 s increased from 0.23 ± 0.01 to 0.38 ± 0.001 spike/s (Figure 3E,F of the Supporting Information). Thus, the viral infection has been shown to have small effects on the rates of secretion, consistent with previous studies (*45*).

Next, chromaffin cells were infected with either the control construct pSFV-GFP, the pSFV Nif-insensitive $\alpha_1$1.2, or the $\alpha_1$1.2/L775P mutant. A 10 s depolarization pulse of 60 mM KCl (K60) elicited significant secretion in pSFV-GFP-infected cells (Figure 4A, left). The addition of 5 μM Nif to the external solution reduced the amperometric spike frequency to ∼2−3 spikes/cell (Figure 4A, middle, and Table 1). The robust inhibition seen by Nif is consistent with the predominant role of Cav1.2 in mediating catecholamine release in native bovine chromaffin cells (see Figure 3) (*40, 41, 44*). In the absence of K60 or in nominally Ca^{2+}-free solution, no amperometric currents were detected (Figure 4A, right).

Depolarization of Nif-insensitive $\alpha_1$1.2-infected cells in the presence of 5 μM Nif revealed single-vesicle release events, which were nearly identical to those seen in the GFP-infected control cells (Figure 4B). Likewise, cells infected with the Nif-insensitive $\alpha_1$1.2/L775P elicited a similar pattern of amperometric currents despite its Ca^{2+} impermeability (Figure 4C).

Applying 200 μM Cd^{2+} to the cells obliterated secretion mediated by either $\alpha_1$1.2 or $\alpha_1$1.2/L775P (Figure 4D). This sensitivity to Cd^{2+}, which binds to the selectivity filter (*46*), is consistent with the accessibility of the pore created by $\alpha_1$1.2/L775P to extracellular ions and the ability of the Ca^{2+}-impermeant channel to trigger secretion.

These results support the view that the initial binding of Ca^{2+} ions at the selectivity filter is sufficient to trigger release, prior to cell entry (*15*−*17*).

Kinetics of Catecholamine Release Supported by the L775P Mutated Channel. We estimated the overall time course of secretion using the normalized waiting time distributions which were constructed by spike counting of GFP-, $\alpha_1$1.2-, and $\alpha_1$1.2/L775P-infected cells (Figure 4E). Because event frequency varies between cells, spike frequencies were quantified for individual cells and then averaged to obtain a cell mean.

The rate of secretion almost overlaps with the maximal slope of the corresponding cumulative spike plots (*47*). The initial rate measured over 12 s after K60 stimulation, seen in noninfected cells, was slightly higher than in the pSFV-infected cells (Table 1). Initial rates of GFP- and $\alpha_1$1.2-infected cells were virtually identical and were 25% faster than in $\alpha_1$1.2/L775P-infected cells (Figure 4F, top). Subsequent to the initial period, catecholamine continued to be released in a sustained manner (Figure 4E,F, bottom). A measure of the sustained frequency of fusion events is provided by the maximal slope of the cumulative spike traces recorded in the time range of 23−40 s (Figure 4F, bottom). Cells infected with $\alpha_1$1.2 had a <20% lower frequency compared to GFP-infected cells, and $\alpha_1$1.2/L775P displayed an additional decrease (22%) in the sustained rate.

The reduction in the initial rate (∼25%) and the more considerable reduction in the sustained rate of secretion

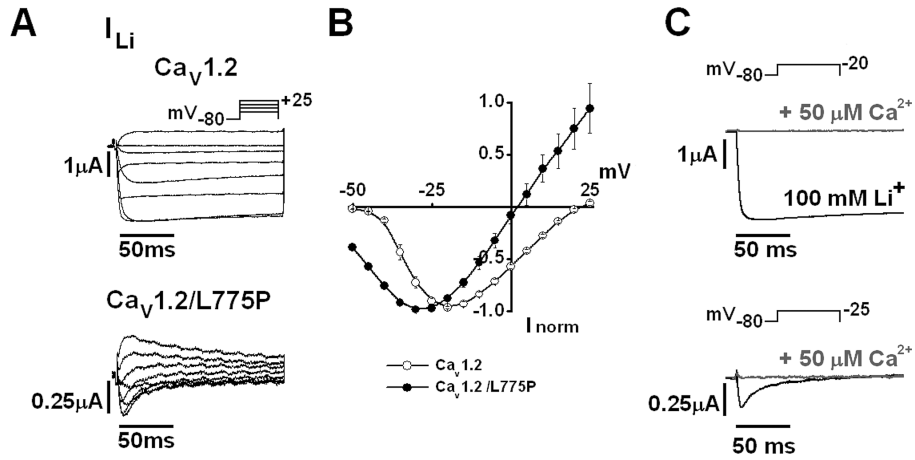

FIGURE 2: Kinetics of I_{Li} through Cav1.2 and mutant L775P channel. (A) Li^+ currents. I_{Li} was evoked in *Xenopus* oocytes expressing $\alpha_1$1.2/α2δ/β2A or $\alpha_1$1.2/L775P/α2δ/β2A by 200 ms pulses from a holding potential of −80 to 25 mV, in 100 mM LiCl, 10 mM EDTA, 14 mM TEA, and 10 mM HEPES (pH 7.5). (B) Voltage dependency. Normalized peak current−voltage relationships of $\alpha_1$1.2/α2δ/β2A [Cav1.2; $n = 12$ (○)] and $\alpha_1$1.2/L775P/α2δ/β2A. Currents were elicited by 200 ms to various test potentials in 5 mV increments [$n = 12$ (●)]. Two sample Student's t tests were applied, and p values of <0.001 were obtained from the two-tailed tests. (C) Ca^{2+} binding at the pore. Superposition of current traces of I_{Li} through Cav1.2 and Cav1.2/L775P elicited from −80 mV to −20 and −25 mV, respectively, in the absence and presence of 50 μM Ca^{2+} applied to the bath (see the legend of Figure 1C for cRNA amounts injected per oocyte). Data collected from oocytes ($n = 12-15$).

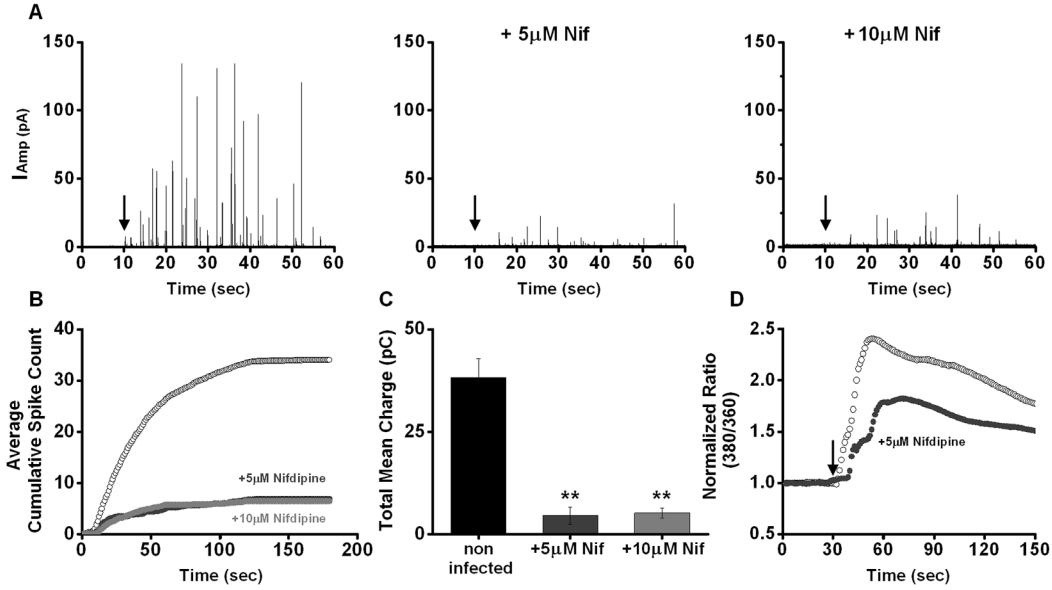

FIGURE 3: Depolarization-evoked catecholamine release in bovine chromaffin cells is nifedipine-sensitive. (A) Amperometric currents from bovine chromaffin cells were triggered by a 10 s puff of K60 (arrow) in the absence (left) and in the presence of 5 (middle) or 10 μM nifedipine (right). (B) Cumulative spike count (spikes >10 pA peak) per cell plotted vs time after K60 depolarization in cells without (○) and with 5 (●) or 10 μM nifedipine (gray circles). Data were collected from 52, 11, and 20 cells, respectively. (C) Total release of catecholamine, quantified by averaging of the total mean charge (TMC) by summation of spike areas in cells without and with 5 or 10 μM nifedipine, as indicated. Asterisks indicate a p of <0.001. (D) Increase in fura-2 imaging during membrane depolarization. Cells had been loaded for 30 min with 3 μM fura-2 washed extensively and stimulated with 60 mM KCl for 10 s (arrow) with and without 5 μM nifedipine in solutions as indicated (see Materials and Methods). Results are expressed as the ratio of fluorescence at 350 nm to that at 380 nm. Traces are representative of four or five single cells present in the same microscope field.

(32%), seen with the Ca^{2+}-impermeable channel, indicate that elevated $[Ca^{2+}]_i$ subsequent to ion permeation is involved in additional steps, which are essential for optimizing the overall release process.

To assess total catecholamine release, we examined the total mean charge (TMC) of the amperometric spikes. TMC was calculated by the summation of spike area from each cell and then averaging over the number of cells. The TMC in GFP-infected cells was strongly inhibited by 5 μM Nif, consistent with the major role of Cav1.2 in supporting catecholamine secretion in bovine chromaffin cells. The TMC values of Nif-insensitive $\alpha_1$1.2 and $\alpha_1$1.2/L775P in the presence of nifedipine did not differ significantly from those seen in the GFP-infected cells without nifedipine (Figure 4G and Table 1).

Kinetic Properties of Spike and Foot Parameters Elicited by L775P Mutated Channel. We then quantified the amperometric currents, analyzing the distribution of the data depicted as cumulative probability (Figure 5A−D). For every parameter, the values from each cell were averaged and presented as the mean of cell averages ± the standard error of the mean (SEM) for each group (*48*). The resulting mean distribution reveals insignificant changes in mean peak area and mean half-width; $\alpha_1$1.2 and $\alpha_1$1.2/L775P exhibited a

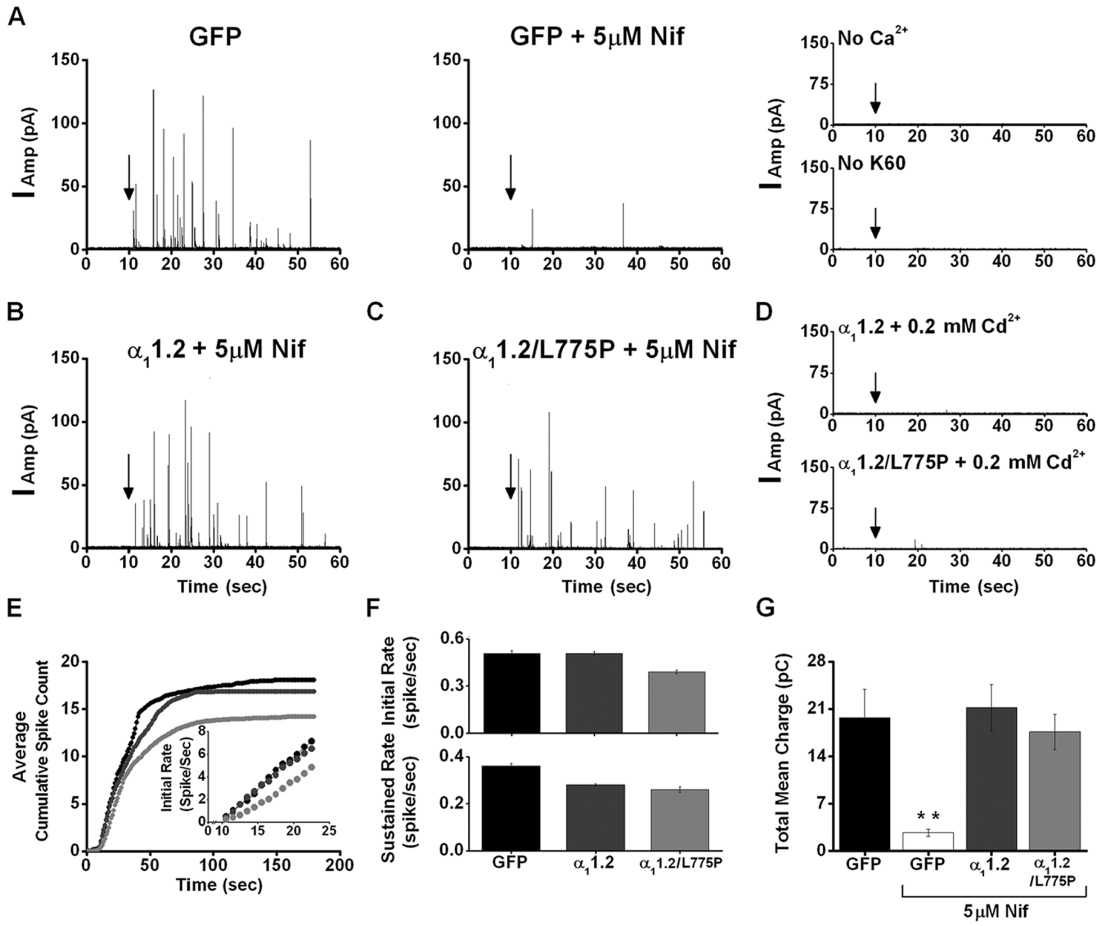

FIGURE 4: Ca^{2+}-impermeable Cav1.2/L775P channel supports depolarization-evoked secretion when expressed in bovine chromaffin cells. (A) Amperometric currents from cells infected with pSFV-GFP in the absence (left) and presence of 5 μM nifedipine (middle). Discrete spikes were triggered by a 10 s puff of K60 (arrow). Stimulation in the absence of K60, or in nominally Ca^{2+}-free solution (right). (B) Amperometric spikes triggered in the presence of 5 μM nifedipine, in cells infected with $\alpha_1$1.2 and (C) $\alpha_1$1.2/L775P (middle). (D) Amperometric spikes of Nif-insensitive $\alpha_1$1.2 or $\alpha_1$1.2/L775P in the presence of 200 μM Cd^{2+} added to the bath solution. (E) Cumulative spike count (spikes >10 pA peak) per cell plotted vs time after K60 depolarization, in cells infected with GFP (●), $\alpha_1$1.2 (dark gray circles), and $\alpha_1$1.2/L775P (light gray circles). Data were collected from 45 to 54 cells and five to eight independent infections for each virus preparation (Table 1). The inset shows an expanded view of the initial cumulative spike counts. (F) The initial rate of secretion corresponds to the initial slope of the cumulative spike count during the first 12 s after the K60 stimulation, in GFP-infected cells, $\alpha_1$1.2, and $\alpha_1$1.2/L775P (top) (Table 1). The sustained rate corresponds to the slope of the cumulative spike count (spike frequency between 23 and 40 s), in GFP-infected cells, $\alpha_1$1.2, and $\alpha_1$1.2/L775P (lower). (G) Total release of catecholamine quantified by averaging of total mean charge (TMC) in GFP-infected cells, $\alpha_1$1.2, and $\alpha_1$1.2/L775P. TMC for GFP-infected cells without and with 5 μM Nif for $\alpha_1$1.2 and α1.1.2/L775P infected cells was calculated by the summation of spike areas. Asterisks indicate a p of <0.005 relative to the GFP-infected cells.

Table 1: Rate Constants and Total Catecholamine Secretion in Non-Infected and GFP-, $\alpha_1$1.2-, and $\alpha_1$1.2/L775P-Infected Bovine Chromaffin Cells

	kinetic parameters of secretion			
cells	no. of spikes per cell	initial rate (spike/s)	sustained rate (spike/s)	total mean charge (pC)
noninfected	20.1	0.76 ± 0.02	0.23 ± 0.01	19.1 ± 2
with GFP	16.13	0.57 ± 0.02	0.36 ± 0.01	19.7 ± 6.2
with GFP and 5 μM Nif	2.3	–	–	2.5 ± 0.2[a]
with $\alpha_1$1.2 and 5 μM Nif	14.98	0.51 ± 0.01	0.28 ± 0.004	15.0 ± 3
with $\alpha_1$1.2/L775P and 5 μM Nif	12.13	0.39 ± 0.01	0.19 ± 0.01	12.1 ± 1.2

[a] p < 0.005 relative to GFP-infected cells.

slightly higher mean peak amplitude, and $\alpha_1$1.2/L775P had lower mean rise time (50−90%) (Figure 5A−D, insets, and Table 1 of the Supporting Information).

The amperometric spikes are often (>80%) preceded by a prespike current event (foot) corresponding to the open state of the fusion pore (*38, 49*). Foot amplitude relates directly to the size of the fusion pore, while foot width indicates stability of the fusion pore (*16, 47*). The mean foot amplitude, mean foot charge, and mean foot width were virtually identical in cells infected with GFP, $\alpha_1$1.2, and $\alpha_1$1.2/L775P (Figure 5E−G and Table 2 of the Supporting Information). As an additional test of foot stability, we determined the mean foot lifetime (τ_{fp}), which depends only on the closing and dilating rate constants (*47*). The mean open times of the fusion pores of noninfected, $\alpha_1$1.2-infected, and GFP-infected cells were indistinguishable (Figure 5H and Table 2 of the Supporting Information). $\alpha_1$1.2/L775P-infected cells exhibited a slight reduction (~15%) in the

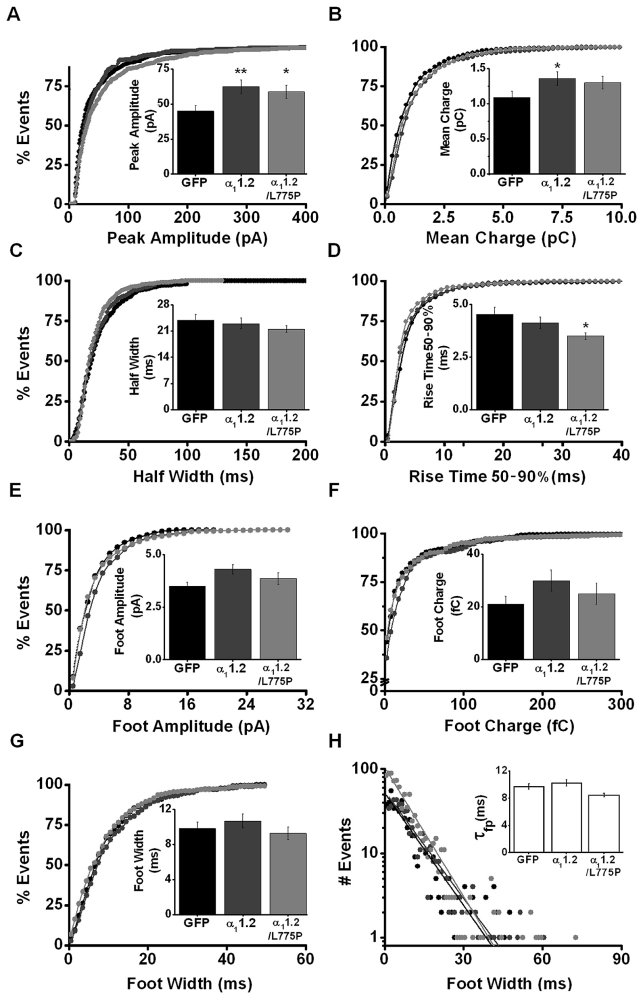

FIGURE 5: Quantitative analysis of amperometric spike and "foot" parameters in Cav1.2/L775P-infected cells. Amperometric spike kinetics. For every parameter, the values from each cell were averaged and presented as the mean of cell averages ± SEM for each group, assigning the same weight to each cell, regardless of the total number of spikes (*48*). Averaged cumulative distributions of (A) peak amplitude (inset, average peak amplitude in GFP, $\alpha_1$1.2, and α_1.1.2/L775P), (B) charge (inset, average charge), (C) half-width (inset, average half-width), and (D) rise time (50−90%) [inset, average rise time (see values in Table 2 of the Supporting Information)]. Kinetic parameters of foot parameters, Cumulative distribution plot of the percent of foot events (right) and analysis of the mean values (left) of (E) foot amplitude, (F) foot charge, and (G) foot width. (H) Distributions of fusion pore open times. Single-exponential fits to time distribution yielded the mean fusion pore open times (τ_{fp}) in GFP-infected ($R^2 = 0.93$), $\alpha_1$1.2-infected ($R^2 = 0.94$), and α_1.1.2/L775P-infected cells ($R^2 = 0.97$). Foot and τ_{fp} values (Table 3 of the Supporting Information). One asterisk indicates a p of < 0.05 vs GFP-infected cells; two asterisks indicate a p of <0.005 vs GFP-infected cells.

mean open time (Figure 5H and Table 2 of the Supporting Information). Hence, the secretion mediated by the Ca^{2+}-impermeable channel affects neither the stability nor the size of the fusion pore, demonstrating a practically normal mode of vesicle fusion properties.

DISCUSSION

In this study, we show that Ca^{2+} interaction at the pore of the channel can trigger secretion prior to Ca^{2+} binding to intracellular proteins. We suggest that voltage-driven perturbations at the Ca^{2+}-bound cavity extend to exocytotic proteins preassembled with the channel and trigger secretion (*15*−*17*, *20*, *22*, *25*, *27*). More specifically, the Ca^{2+} channel acts as a signaling molecule prior to the transport of Ca^{2+} into the cell. Such signaling is feasible in view of the wide-ranging readjustments of protein atoms, likely to occur during ion binding, similar to what is seen at the K^+ channel selectivity filter, which extends 15 Å from the ion pathway (*50*).

Previously, we postulated that the static change caused by ion binding at the filter, which is governed by the ion affinity at the filter ($K_d = k_{off}/k_{on}$) and diffusion coefficient of Ca^{2+}, is an essential precondition for triggering secretion (*15*, *17*). We proposed that La^{3+} binding at the Cav1.2 selectivity filter, although different from divalent ion binding at the pore, conveys a "releasing" conformation. We also showed that Ca^{2+}, Sr^{2+}, Ba^{2+}, La^{3+}, and to a small degree also Ce^{3+} and Pr^{3+} matched the required ion size for conferring a releasing mode, while metals with smaller ionic radii, Cd^{2+}, Nd^{3+}, Eu^{3+}, and Gd^{3+}, did not (*15*).

To extend these studies, we used a molecular approach to test the ability of a Ca^{2+}-impermeable mutated $\alpha_1$1.2 channel subunit to mediate secretion during membrane depolarization.

We utilized an $\alpha_1$1.2/L775P subunit that is expressed and targeted to the cell membrane but is Ca^{2+}-impermeable (*30*) (results presented here). The slight Li^+ permeability of $\alpha_1$1.2/L775P has demonstrated that the mutated channel retains its voltage sensitivity and could be opened during membrane depolarization. Inhibition of I_{Li} by 50 μM Ca^{2+} indicated that Ca^{2+} ion was bound at the pore (*10*).

The unique coupling of Cav1.2 to the release apparatus in bovine chromaffin cells provided a tool for studying secretion mediated by the impermeable $\alpha_1$1.2/L775P subunit. Secretion could be distinguished from secretion through endogenous channels by a single-point mutation rendering the channel insensitive to nifedipine (*35*). The $\alpha_1$1.2/L775P mutant mediated catecholamine release in response to K60 stimulation, in the presence of 5 μM nifedipine. At this concentration, nifedipine inhibits 85−90% of the release mediated by the endogenous channels. This result showed for the first time that evoked release could be triggered by Ca^{2+} binding at Ca^{2+}-impermeable channel. The essential role of Ca^{2+} binding at the pore in triggering secretion was confirmed also by the Cd^{2+} block of secretion, via binding at the L775P selectivity filter.

The ~25% slower rate of secretion mediated by the mutated channel implied that Ca^{2+} influx and subsequent binding to synaptotagmin, a step missing in secretion mediated by the Ca^{2+}-impermeable channel, contribute to optimization of the vesicle fusion process.

The commonly accepted view of the conductance of current through the VGCC is that a conducting channel is a pore occupied by two Ca^{2+} ions, whereas a pore occupied by a single Ca^{2+} ion is nonconducting (*10*). This was further implied by suggesting that nifedipine stabilized a channel conformation that holds a single Ca^{2+} ion at the pore, generating a nonconducting channel (*24*, *51*).

We propose a schematic model that connects the coupling of transitions between a nonconducting and conducting pore to the ability of the channel to support release (Figure 6). Accordingly, ion relocation within the selectivity filter, which converts a single-ion (high affinity) to a double-ion occupancy pore (low affinity) and leads to a transition from a

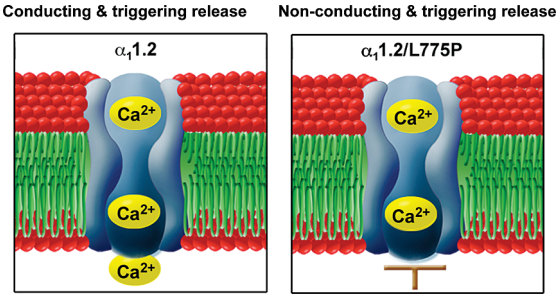

FIGURE 6: Schematic view of Ca^{2+} binding at the channel cavity and the effect on current conductance and depolarization-induced secretion. Cav1.2 channels readily transport Ca^{2+} through the selectivity filter, which constitutes the selectivity filter. The EEEE locus occupancy by a second ion drives Ca^{2+} influx (top). Cav1.2/L775P that binds Ca^{2+} at the selectivity filter allows residency of two Ca^{2+} ions, which drives secretion without conduction (bottom). Nifedipine stabilizes the selectivity filter in a conformation that is analogous to a pore occupied by a single Ca^{2+} ion (*51*). We suggest that the movement of Ca^{2+} from high affinity (single ion occupancy) to low affinity (two ions occupancy) confers a 'conducting' conformation that appears to coinside with a releasing conformation.

nonconducting to a conducting channel, is also the switch that triggers release. This step precedes and is independent of Ca^{2+} influx. The pore of the L775P mutant appears to allow double-ion occupancy, similar to that of the wild-type channel, because it could trigger secretion in response voltage perturbations (Figure 6). The acquired releasing conformation directs a signal from the channel, most likely to the transmembrane of syntaxin 1A, and to the exocytotic machinery, to trigger release (*20, 27, 29, 52, 53*).

Consistent with the proposed model, the Ca^{2+} channel is acting as the Ca^{2+} sensor protein of depolarization-evoked catecholamine secretion in chromaffin cells. In fact, the proposed model could also account for the physiological trigger of the fast ($\sim$100 μs) process of synaptic transmission, because conformational changes occur on a similar time scale. In addition, this model predicts that spontaneous release would occur whenever the pore switches from single-ion to double-ion occupancy.

These results do not dispute the existence of subsequent effects of $[Ca^{2+}]_i$ on the overall secretory process, e.g., recruitment and docking of vesicles, but rather they suggest that the initial trigger of secretion is the relocation of Ca^{2+} ions within sites at the selectivity filter, enabled during membrane depolarization. Therefore, the VGCC could be the putative Ca^{2+} sensor protein that acts prior to binding of intracellular Ca^{2+} to cytosolic proteins.

MATERIALS AND METHODS

Mutagenesis. The complete cDNAs of the $\alpha_1$1.2 subunit (rabbit) (dN60-del1773; GenBank entry X15539) and rat β2A (m80545) were kindly donated by N. Qin and L. Birnbaumer (University of North Carolina, Chapel Hill, NC) (*54*). α2/δ rabbit skeletal (GenBank entry M21948) was from A. Schwartz (University of Ohio, Athens, OH). The α1 subunit in-frame 5′ to the coding region of a modified green fluorescent protein (GFP) was from M. Grabner; $\alpha_1$1.2/L775P was from S. Hering. A modified pSFV1 (Invitrogen) plasmid where an internal ribosome entry site from polio virus had been inserted followed by the gene for enhanced GFP was from U. Ashery. For amperometry studies, plasmids lacking the GFP tag, $\alpha_1$1.2/T1066Y and $\alpha_1$1.2/L775P/T1066Y, were inserted upstream of the internal ribosome entry site using *Bam*HI and *Bss*HII restriction sites. All constructs were verified by DNA sequencing.

Expression in Xenopus Oocytes and cRNA Injection. Stage V−VI *Xenopus laevis* oocytes were removed surgically from the ovaries of anesthetized animals and transferred to a Ca^{2+}-free medium [96 mM NaCl, 2 mM KCl, 1 mM $MgCl_2$, and 5 mM HEPES (pH 7.4)] containing 1 mg/mL collagenase (253 units/mg) (Wortington Biochemical Corp.). The follicular cell layer was removed by shaking the oocytes in this buffer for 1.5−2 h at room temperature. After being extensively washed, the oocytes were transferred to ND96 buffer [96 mM NaCl, 3 mM KCl, 1 mM $MgCl_2$, 1.8 mM $CaCl_2$, and 5 mM HEPES (pH 7.4)] containing 2.5 mM pyruvate, 100 units/mL penicillin, and 10 μg/mL streptomycin at 12−20 h before cRNA injection. Oocytes were maintained in the ND96 buffer with daily buffer exchange.

Injection of cRNA onto Oocytes and Electrophysiology. cRNAs were prepared using the T7 Invitrogen transcription kit, and the product was monitored by gel electrophoresis and optical density measurements. In vitro transcribed capped cRNA of the channel subunits was injected into the defolliculated oocytes in a final volume of 40 nL using a Drummond 510 (Broomall, PA) microinjector. cRNA mixtures encoding Ca^{2+} channel subunits were adjusted empirically to make the inward current <4 μA. Barium currents (I_{Ba}), calcium currents (I_{Ca}), and lithium currents (I_{Li}) through voltage-gated Ca^{2+} channels were recorded in *Xenopus* oocytes at 22 °C 5 days after injection using the standard two-microelectrode voltage clamp (*15*).

Whole-cell voltage clamp recordings were obtained from oocytes 5 days after cRNA injection, as described previously (*15*). To minimize Ca^{2+}-activated Cl^- currents, oocytes were injected with BAPTA (final concentration of 5 mM) prior to recordings. Membrane currents were recorded by a two-electrode voltage clamp method using a TEV-200A amplifier (Dagan). Bath solution contained 10 mM $Ca(OH)_2$ or 10 mM $Ba(OH)_2$, 50 mM *N*-methyl-D-glucamine, 1 mM KOH, 40 mM tetraethylammonium, and 5 mM HEPES titrated to pH 7.5 with methanesulfonic acid CH_3SO_3H. Li^+ currents were elicited in a solution containing 100 mM LiCl, 10 mM EDTA, 14 mM tetraethylammonium, and 10 mM HEPES titrated to pH 7.4 with methanesulfonic acid. Current traces were leak-subtracted online with Clampex 8.2, and channel activation rates were analyzed by applying a monoexponential fit (Axon Instruments, Foster City, CA) to the current traces in the relevant ranges.

Data Presentation and Statistical Analysis. Peak current and time constant values were analyzed by Clampfit 9.0 and transferred as an ASCI file to an Excel worksheet (Microsoft Inc.). Data were averaged for each group of oocytes, and the standard error (SE) was determined. Data are presented as means ± SE. Statistical significance relative to the control group in each experiment was determined by a Student's *t* test with Excel. Statistical significance between multiple groups in each experiment was determined using a one-way analysis of variance test using Origin 6 (Microcal). Final data were transferred to an Origin 6 worksheet, plotted, and printed as final figures.

Chromaffin Cell Preparation and Culture. Bovine adrenal glands were obtained at a local slaughterhouse. The adrenal

medulla cells were isolated as described previously (*15*), cultured, and plated at a density of 5×10^4 cells/cm^2 on glass coverslips placed in 35 mm plates, in DMEM (Gibco) supplemented with ITS-X (Sigma). Cells were incubated at 37 °C in 5% CO_2 and used for amperometric recordings 2−4 days after preparation at 23 °C.

Amperometric Recordings of the Release of Catecholamine from Chromaffin Cells. Amperometry recordings were carried out using 5 μm thin carbon fiber electrodes (CFE ALA Inc., Westbury, NY) and a VA-10 amplifier (NPI-electronic, Tamm, Germany) held at 800 mV as described previously (*38*). Cells were rinsed three or four times prior to the experiment and bathed during the recordings at 23 °C in an iso-osmotic physiological solution [149 mM NaCl, 2 mM KCl, 1 mM $MgCl_2$, 2 mM $CaCl_2$, 10 mM glucose, and 10 mM HEPES (pH 7.3) at ~23 °C (adjusted with NaOH)]. Individual cells were stimulated to release by a 10 s application of iso-osmotic 60 mM KCl buffer from an ~3 μm tipped micropipette placed 30 μm from the cell in the bath. Amperometric currents were sampled at 10 kHz, using Clampex 9.0 (Axon Instruments), and low-pass-filtered at 3 kHz.

Secretion of catecholamines from fluorescent cells identified with 480 nm excitation was recorded 10−16 h after infection by amperometry.

pSFV Virus Preparation and Infection. Recombinant SFV particles were generated as described previously (*45*). Briefly, in vitro transcribed RNA from pSFV-GFP, or pSFV expressing GFP through an internal ribosome entry site (IRES) motif, pSFV-Nif-insensitive $\alpha_1$1.2-IRES-GFP, or pSFV-Nif-insensitive $\alpha_1$1.2/L775P-IRES-GFP was co-electroporated into BHK-21 cells with pSFV-Helper 2 RNA. Virus stocks were harvested 24 h later and activated with α-chymotrypsin before infection studies. Approximate titers were estimated by infection of known numbers of BHK-21 cells with serial dilutions of SFV stocks, and the GFP-positive cells were counted. Generally, titers in the range of 5×10^8 infectious particles/mL were obtained.

SFV particle titers (30 μL/dish) were performed on cultured cells (2×10^5 cells per dish) 5−48 h after plating. Infected cells were identified by their GFP fluorescence.

Acquisition and Analysis of Amperometric Data. Rates of secretion were determined for individual cells and averaged. The initial (10−22 s) and sustained (23−40 s) rates of secretion were determined from the slopes of the corresponding cumulative spike plots. Data were analyzed as described in the text and figure legends. Error bars give standard errors. Spikes exceeding 3 times the background noise (>10 pA) were analyzed. All peaks identified by the program were inspected visually, and bad signals were excluded manually.

Free Intracellular Ca^{2+} Concentration Measurements. The intracellular Ca^{2+} concentration ($[Ca^{2+}]_i$) was estimated by fura-2 microfluorometry of single chromaffin cells (*55*). Intact chromaffin cells plated on glass coverslips were incubated with 3 μM fura-2-acetoxymethylester (fura-2-AM) at 37 °C for 45 min before being washed three times with 0 Ca^{2+}-iso-osmotic solution. Intracellular fura-2 bound to Ca^{2+} was excited at 350 nm, while free fura-2 was excited at 380 nm using a digital CCD camera (PCD Sensicam CCD, oil lens 63× NA 1.5) and analyzed with Image J. The ratio of the emission at 350 nm and to excitation at 380 nm was determined. The imaging system was a Zeiss Axiovert 34 microscope coupled to a Till photonics system. On each coverslip, four or five chromaffin cells were selected and individually imaged. Image pairs (one at 350 and 380 nm) were obtained every second for 200 s. KCl (60 mM) was added 30 s after fluorescence monitoring had begun. The 350 nm image was divided by the 380 nm image to provide a ratiometric image.

Confocal Imaging. Single optical sections through the oocytes were acquired with an Olympus FV1000 camera equipped with a 40× oil objective (NA 1.3). A 488 nm excitation laser with narrow-band emission filters of 505−525 nm in the GFP channel was used. Sequential scanning was performed with a resolution set to 512 × 512 pixels (0.621 μm/pixel), and single optical sections ~0.5 μm thick were captured. The exposure time was 8 μs/pixel.

ACKNOWLEDGMENT

Thanks to Dr. M. Trus for discussions and editing of the manuscript.

SUPPORTING INFORMATION AVAILABLE

Kinetic analysis of GFP-tagged Cav1.2 and Cav1.2/T1066Y channels expressed in *Xenopus* oocytes (Figure 1), nifedipine sensitivity of Cav1.2 and nifedipine insensitivity of Cav1.2/T1066Y (Figure 2), amperometry kinetics of uninfected and SFV-GFP-infected bovine chromaffin cells (Figure 3), and spike parameters (Table 1) and foot parameters (Table 2) of noninfected and GFP-, $\alpha_1$1.2-, and $\alpha_1$1.2/L775P-infected bovine chromaffin cells. This material is available free of charge via the Internet at http://pubs.acs.org.

REFERENCES

1. Katz, B., and Miledi, R. (1969) Spontaneous and evoked activity of motor nerve endings in calcium Ringer. *J. Physiol. 203*, 689–706.
2. Geppert, M., Goda, Y., Hammer, R. E., Li, C., Rosahl, T. W., Stevens, C. F., and Sudhof, T. C. (1994) Synaptotagmin I: A major Ca^{2+} sensor for transmitter release at a central synapse. *Cell 79*, 717–727.
3. Fernandez-Chacon, R., Konigstorfer, A., Gerber, S. H., Garcia, J., Matos, M. F., Stevens, C. F., Brose, N., Rizo, J., Rosenmund, C., and Sudhof, T. C. (2001) Synaptotagmin I functions as a calcium regulator of release probability. *Nature 410*, 41–49.
4. Voets, T., Moser, T., Lund, P. E., Chow, R. H., Geppert, M., Sudhof, T. C., and Neher, E. (2001) Intracellular calcium dependence of large dense-core vesicle exocytosis in the absence of synaptotagmin I. *Proc. Natl. Acad. Sci. U.S.A. 98*, 11680–11685.
5. Sorensen, J. B., Fernandez-Chacon, R., Sudhof, T. C., and Neher, E. (2003) Examining synaptotagmin 1 function in dense core vesicle exocytosis under direct control of Ca^{2+}. *J. Gen. Physiol. 122*, 265–276.
6. Jahn, R., and Sudhof, T. C. (1999) Membrane fusion and exocytosis. *Annu. Rev. Biochem. 68*, 863–911.
7. Wang, C. T., Grishanin, R., Earles, C. A., Chang, P. Y., Martin, T. F., Chapman, E. R., and Jackson, M. B. (2001) Synaptotagmin modulation of fusion pore kinetics in regulated exocytosis of dense-core vesicles. *Science 294*, 1111–1115.
8. Lynch, K. L., Gerona, R. R., Larsen, E. C., Marcia, R. F., Mitchell, J. C., and Martin, T. F. (2007) Synaptotagmin C2A loop 2 mediates Ca^{2+}-dependent SNARE interactions essential for Ca^{2+}-triggered vesicle exocytosis. *Mol. Biol. Cell 18*, 4957–4968.
9. Chapman, E. R. (2008) How Does Synaptotagmin Trigger Neurotransmitter Release? *Annu. Rev. Biochem. 77*, 615–641.
10. Sather, W. A., and McCleskey, E. W. (2003) Permeation and selectivity in calcium channels. *Annu. Rev. Physiol. 65*, 133–159.

11. Kim, M. S., Morii, T., Sun, L. X., Imoto, K., and Mori, Y. (1993) Structural determinants of ion selectivity in brain calcium channel. *FEBS Lett. 318*, 145–148.
12. Mikala, G., Bahinski, A., Yatani, A., Tang, S., and Schwartz, A. (1993) Differential contribution by conserved glutamate residues to an ion-selectivity site in the L-type Ca^{2+} channel pore. *FEBS Lett. 335*, 265–269.
13. Tang, S., Mikala, G., Bahinski, A., Yatani, A., Varadi, G., and Schwartz, A. (1993) Molecular localization of ion selectivity sites within the pore of a human L-type cardiac calcium channel. *J. Biol. Chem. 268*, 13026–13029.
14. Yang, J., Ellinor, P. T., Sather, W. A., Zhang, J. F., and Tsien, R. W. (1993) Molecular determinants of Ca^{2+} selectivity and ion permeation in L-type Ca^{2+} channels. *Nature 366*, 158–161.
15. Lerner, I., Trus, M., Cohen, R., Yizhar, O., Nussinovitch, I., and Atlas, D. (2006) Ion interaction at the pore of Lc-type Ca^{2+} channel is sufficient to mediate depolarization-induced exocytosis. *J. Neurochem. 97*, 116–127.
16. Marom, M., Sebag, A., and Atlas, D. (2007) Cations Residing at the Selectivity Filter of the Voltage-Gated Ca^{2+}-Channel Modify Fusion-Pore Kinetics. *Channels 1* (5), 377–386.
17. Trus, M., Corkey, R. F., Nesher, R., Richard, A. M., Deeney, J. T., Corkey, B. E., and Atlas, D. (2007) The L-type Voltage-Gated Ca^{2+} Channel Is the Ca^{2+} Sensor Protein of Stimulus-Secretion Coupling in Pancreatic Beta Cells. *Biochemistry 46*, 14461–14467.
18. Bezprozvanny, I., Scheller, R. H., and Tsien, R. W. (1995) Functional impact of syntaxin on gating of N-type and Q-type calcium channels. *Nature 378*, 623–626.
19. Wiser, O., Tobi, D., Trus, M., and Atlas, D. (1997) Synaptotagmin restores kinetic properties of a syntaxin-associated N-type voltage sensitive calcium channel. *FEBS Lett. 404*, 203–207.
20. Wiser, O., Trus, M., Hernandez, A., Renstrom, E., Barg, S., Rorsman, P., and Atlas, D. (1999) The voltage sensitive Lc-type Ca^{2+} channel is functionally coupled to the exocytotic machinery. *Proc. Natl. Acad. Sci. U.S.A. 96*, 248–253.
21. Wiser, O., Cohen, R., and Atlas, D. (2002) Ionic dependence of Ca^{2+} channel modulation by syntaxin 1A. *Proc. Natl. Acad. Sci. U.S.A. 99*, 3968–3973.
22. Tobi, D., Wiser, O., Trus, M., and Atlas, D. (1998) N-Type voltage-sensitive calcium channel interacts with syntaxin, synaptotagmin and SNAP-25 in a multiprotein complex. *Receptors Channels 6*, 89–98.
23. Zhang, J. F., Ellinor, P. T., Aldrich, R. W., and Tsien, R. W. (1994) Molecular determinants of voltage-dependent inactivation in calcium channels. *Nature 372*, 97–100.
24. Catterall, W. A. (1999) Interactions of presynaptic Ca^{2+} channels and snare proteins in neurotransmitter release. *Ann. N.Y. Acad. Sci. 868*, 144–159.
25. Atlas, D., Wiser, O., and Trus, M. (2001) The voltage-gated Ca^{2+} channel is the Ca^{2+} sensor of fast neurotransmitter release. *Cell. Mol. Neurobiol. 21*, 717–731.
26. Atlas, D. (2001) Functional and physical coupling of voltage-sensitive calcium channels with exocytotic proteins: Ramifications for the secretion mechanism. *J. Neurochem. 77*, 972–985.
27. Trus, M., Wiser, O., Goodnough, M. C., and Atlas, D. (2001) The transmembrane domain of syntaxin 1A negatively regulates voltage-sensitive Ca^{2+} channels. *Neuroscience 104*, 599–607.
28. Cohen, R., and Atlas, D. (2004) R-type voltage-gated Ca^{2+} channel interacts with synaptic proteins and recruits synaptotagmin to the plasma membrane of *Xenopus* oocytes. *Neuroscience 128*, 831–841.
29. Cohen, R., Marom, M., and Atlas, D. (2007) Depolarization-Evoked Secretion Requires Two Vicinal Transmembrane Cysteines of Syntaxin 1A. *PLoS One 2*, e1273.
30. Hohaus, A., Beyl, S., Kudrnac, M., Berjukow, S., Timin, E. N., Marksteiner, R., Maw, M. A., and Hering, S. (2005) Structural determinants of L-type channel activation in segment IIS6 revealed by a retinal disorder. *J. Biol. Chem. 280*, 38471–38477.
31. Schonn, J. S., Maximov, A., Lao, Y., Sudhof, T. C., and Sorensen, J. B. (2008) Synaptotagmin-1 and -7 are functionally overlapping Ca^{2+} sensors for exocytosis in adrenal chromaffin cells. *Proc. Natl. Acad. Sci. U.S.A. 105*, 3998–4003.
32. Wiser, O., Bennett, M. K., and Atlas, D. (1996) Functional interaction of syntaxin and SNAP-25 with voltage-sensitive L- and N-type Ca^{2+} channels. *EMBO J. 15*, 4100–4110.
33. Almers, W., McCleskey, E. W., and Palade, P. T. (1984) A non-selective cation conductance in frog muscle membrane blocked by micromolar external calcium ions. *J. Physiol. 353*, 565–583.
34. Kuo, C. C., and Hess, P. (1993) Ion permeation through the L-type Ca^{2+} channel in rat phaeochromocytoma cells: Two sets of ion binding sites in the pore. *J. Physiol. 466*, 629–655.
35. He, M., Bodi, I., Mikala, G., and Schwartz, A. (1997) Motif III S5 of L-type calcium channels is involved in the dihydropyridine binding site. A combined radioligand binding and electrophysiological study. *J. Biol. Chem. 272*, 2629–2633.
36. Dolmetsch, R. E., Pajvani, U., Fife, K., Spotts, J. M., and Greenberg, M. E. (2001) Signaling to the nucleus by an L-type calcium channel-calmodulin complex through the MAP kinase pathway. *Science 294*, 333–339.
37. Wightman, R. M., Jankowski, J. A., Kennedy, R. T., Kawagoe, K. T., Schroeder, T. J., Leszczyszyn, D. J., Near, J. A., Diliberto, E. J., Jr., and Viveros, O. H. (1991) Temporally resolved catecholamine spikes correspond to single vesicle release from individual chromaffin cells. *Proc. Natl. Acad. Sci. U.S.A. 88*, 10754–10758.
38. Chow, R. H., von Ruden, L., and Neher, E. (1992) Delay in vesicle fusion revealed by electrochemical monitoring of single secretory events in adrenal chromaffin cells. *Nature 356*, 60–63.
39. Jankowski, J. A., Schroeder, T. J., Ciolkowski, E. L., and Wightman, R. M. (1993) Temporal characteristics of quantal secretion of catecholamines from adrenal medullary cells. *J. Biol. Chem. 268*, 14694–14700.
40. Cena, V., Nicolas, G. P., Sanchez-Garcia, P., Kirpekar, S. M., and Garcia, A. G. (1983) Pharmacological dissection of receptor-associated and voltage-sensitive ionic channels involved in catecholamine release. *Neuroscience 10*, 1455–1462.
41. Artalejo, C. R., Adams, M. E., and Fox, A. P. (1994) Three types of Ca^{2+} channel trigger secretion with different efficacies in chromaffin cells. *Nature 367*, 72–76.
42. Lopez, M. G., Albillos, A., de la Fuente, M. T., Borges, R., Gandia, L., Carbone, E., Garcia, A. G., and Artalejo, A. R. (1994) Localized L-type calcium channels control exocytosis in cat chromaffin cells. *Pfluegers Arch. 427*, 348–354.
43. Avidor, B., Avidor, T., Schwartz, L., De Jongh, K. S., and Atlas, D. (1994) Cardiac L-type Ca^{2+} channel triggers transmitter release in PC12 cells. *FEBS Lett. 342*, 209–213.
44. Garcia, A. G., Garcia-De-Diego, A. M., Gandia, L., Borges, R., and Garcia-Sancho, J. (2006) Calcium signaling and exocytosis in adrenal chromaffin cells. *Physiol. Rev. 86*, 1093–1131.
45. Ashery, U., Betz, A., Xu, T., Brose, N., and Rettig, J. (1999) An efficient method for infection of adrenal chromaffin cells using the Semliki Forest virus gene expression system. *Eur. J. Cell Biol. 78*, 525–532.
46. Lansman, J. B., Hess, P., and Tsien, R. W. (1986) Blockade of current through single calcium channels by Cd^{2+}, Mg^{2+}, and Ca^{2+}. Voltage and concentration dependence of calcium entry into the pore. *J. Gen. Physiol. 88*, 321–347.
47. Wang, C. T., Bai, J., Chang, P. Y., Chapman, E. R., and Jackson, M. B. (2006) Synaptotagmin-Ca^{2+} triggers two sequential steps in regulated exocytosis in rat PC12 cells: Fusion pore opening and fusion pore dilation. *J. Physiol. 570*, 295–307.
48. Colliver, T. L., Hess, E. J., Pothos, E. N., Sulzer, D., and Ewing, A. G. (2000) Quantitative and statistical analysis of the shape of amperometric spikes recorded from two populations of cells. *J. Neurochem. 74*, 1086–1097.
49. Breckenridge, L. J., and Almers, W. (1987) Currents through the fusion pore that forms during exocytosis of a secretory vesicle. *Nature 328*, 814–817.
50. Lockless, S. W., Zhou, M., and MacKinnon, R. (2007) Structural and thermodynamic properties of selective ion binding in a K^+ channel. *PLoS Biol. 5*, e121.
51. Peterson, B. Z., and Catterall, W. A. (2006) Allosteric interactions required for high-affinity binding of dihydropyridine antagonists to $Ca_V1.1$ channels are modulated by calcium in the pore. *Mol. Pharmacol. 70*, 667–675.
52. Cohen, R., Schmitt, B. M., and Atlas, D. (2005) Molecular identification and reconstitution of depolarization-induced exocytosis monitored by membrane capacitance. *Biophys. J. 89*, 4364–4373.
53. Arien, H., Wiser, O., Arkin, I. T., Leonov, H., and Atlas, D. (2003) Syntaxin 1A modulates the voltage-gated L-type calcium channel ($Ca_v1.2$) in a cooperative manner. *J. Biol. Chem. 278*, 29231–29239.
54. Wei, X., Neely, A., Lacerda, A. E., Olcese, R., Stefani, E., Perez-Reyes, E., and Birnbaumer, L. (1994) Modification of Ca^{2+} channel activity by deletions at the carboxyl terminus of the cardiac $\alpha 1$ subunit. *J. Biol. Chem. 269*, 1635–1640.
55. Grynkiewicz, G., Poenie, M., and Tsien, R. Y. (1985) A new generation of Ca^{2+} indicators with greatly improved fluorescence properties. *J. Biol. Chem. 260*, 3440–3450.

BI801619F